



## Research papers

# The effect of the spatially inhomogeneous wind field on the wave spectra employing an ERS-2 SAR PRI image

Nelson Violante-Carvalho<sup>a,\*</sup>, Ian Robinson<sup>b</sup>, Christine Gommenginger<sup>b</sup>, Luiz Mariano Carvalho<sup>c</sup>, Francisco Ocampo-Torres<sup>d</sup>

<sup>a</sup> Rio de Janeiro State University (UERJ), Faculty of Oceanography—FAOC, R. São Francisco Xavier, Rio de Janeiro 20550-900, Brasil

<sup>b</sup> National Oceanography Centre, Southampton (NOCS), European Way, Southampton SO14 3ZH, United Kingdom

<sup>c</sup> Rio de Janeiro State University (UERJ), Institute of Mathematics and Statistics—IME, Brasil

<sup>d</sup> Centro de Investigación Científica y Educación Superior de Ensenada (CICESE), Km 107 Carretera Tijuana-Ensenada, Ensenada 22860, Mexico

## ARTICLE INFO

## Article history:

Received 24 February 2011

Received in revised form

10 December 2011

Accepted 12 December 2011

Available online 2 February 2012

## Keywords:

SAR wave spectra

ERS-1&2 SAR precision image

Interaction between wind sea and swell

## ABSTRACT

Using wave spectra extracted from image mode ERS-2 SAR scenes, the spatial homogeneity of the wave field in deep water is investigated. From the  $100 \times 100$  km image, several small images of  $6.4 \times 6.4$  km are selected and the wave spectra are computed. The locally disturbed wind velocity pattern, caused by the sheltering effect of large mountains near the coast, translates into the selected SAR image as regions of higher and lower wind speed. Assuming that the swell field is uniform over the whole image, SAR derived swell spectra retrieved from the sheltered and non-sheltered areas are intercompared. Any difference between them could be related to a possible modification associated with the sheltering effect on the wind speed and/or a possible interaction between wind sea and swell, since the wind sea part of the spectrum would be slightly different due to the different wind speeds. The results show that there is no significant modification, and apparently there is no clear difference in the swell spectra despite the different wind sea components and wind speeds.

© 2012 Elsevier Ltd. All rights reserved.

## 1. Introduction

Most of the studies that have examined the effects of long waves (swell) on shorter (wind sea) were carried out in laboratory tanks (for example, Phillips and Banner, 1974; Donelan, 1987), or through numerical simulations (Masson, 1993; Young et al., 1995). Several works seem to indicate that wind waves are attenuated in the presence of long waves, however, there is no consensus regarding the exact causes of the suppression and to what extent.

The nonlinear wave–wave interaction term ( $S_{nl}$ ) in the wave energy equation has been shown to play an important role in the coupling between swell and wind sea causing the attenuation of the shorter waves in the presence of the longer waves in the frequency range just below the peak frequency of the wind sea. The coupling causes the swell to grow at the expense of the wind waves, but it seems to be only significant if swell and wind waves are close in frequency space. The suppression of wind waves by the swell depends on the swell's steepness and also on the relative direction of propagation between swell and wind sea,

where the coupling is, according to numerical experiments, maximum at about  $40^\circ$  (Masson, 1993).

The work by Phillips and Banner (1974) pointed out that the suppression of wind waves is due to enhanced dissipation ( $S_{ds}$  term), which is caused by modulation of the short waves by the long waves. Moreover, their theoretical results predict that wind waves are attenuated by opposing swell, which were not corroborated by other authors. The results presented by Mitsuyasu and Yoshida (2005), for example, point in the opposite direction, with wind waves intensified by an opposing swell.

Chen and Belcher (2000), on the other hand, suggested that the attenuation of wind waves by swell is related to reduction in the magnitude of the wind input source term  $S_{in}$ . They proposed that the swell reduces the momentum from the wind, therefore hampering the development of the wind sea. More recently, the results reported in García-Nava et al. (2009) suggested that in low wind conditions swell increases drag, whereas at higher winds, swell reduces drag from the wind. Therefore, the presence of swell, depending on the wind speed, could slow down or speed up the development of the short waves.

The matter is yet open to discussion, and the interaction is not well investigated in the open ocean where swell is ubiquitous. It is not clear whether or how its presence would change the mechanics of wave growth (Dobson et al., 1989; Hanson and Phillips, 1999; Violante-Carvalho et al., 2004). The main difficulty

\* Corresponding author. Tel.: +55 21 2334 0903.

E-mail addresses: [n\\_violante@uerj.br](mailto:n_violante@uerj.br),

[violante\\_carvalho@yahoo.co.uk](mailto:violante_carvalho@yahoo.co.uk) (N. Violante-Carvalho).

lies in the temporal and spatial scales involved, since any discernible modification of the wave field would take place over a long distance or over a long time. The relatively large area covered by a Synthetic Aperture Radar (SAR) image turns out to become an interesting tool to perform such analysis.

SAR on-board satellites is the only source of directional wave spectra with continuous and global coverage. In SAR image mode the instrument acquires  $100 \times 100$  km images but due to on-board storage limitations it can be operated only with a ground station in sight, with images usually covering coastal areas. The SAR wave mode (SWM), on the other hand, was introduced to overcome this coverage limitation since the much smaller imagerettes are stored on-board and transmitted once per orbit to ground stations. Millions of SWM imagerettes have been acquired since the launch in the early 1990s of the first European Remote Sensing Satellite ERS-1 and its successors ERS-2 and ENVISAT, in general over oceanic areas since both modes of operation cannot operate simultaneously.

Better estimates of the sea state will necessarily require improvements in retrieval schemes. The procedure to extract the directional wave spectrum from SWM is not simple. The main limitation lies in the fact that the SAR ocean wave imaging mechanism is strongly nonlinear due to the radial velocity induced by the waves which causes a Doppler offset in the image plane with smearing and loss of information beyond a high wavenumber cut-off. This problem has been tackled by different methods, such as described by Hasselmann and Hasselmann (1991), Krogstad et al. (1994), Hasselmann et al. (1996), Mastenbroek and de Valk (2000), Schulz-Stellenfleth et al. (2005), and Ardhuin et al. (2009).

Despite the overall consensus about the reliability of wave models, in particular in deep water, in coastal areas numerical models produce relatively large errors. The potential to retrieve the directional wave spectrum over coastal regions using SAR image mode has not yet been fully achieved, with very few papers specifically addressing the problem (see, for example, Collard et al., 2005).

SAR Level-1 products from wave mode of ERS and ENVISAT have exactly the same characteristics as those from image mode of the same instruments, except for varying incidence angle. Most of the image mode data are near coastal regions and therefore the transfer functions need to be adapted to account for the nonlinearities and modified dispersion relation induced by the limited depth. For ENVISAT horizontal–horizontal (HH) polarized data, some modifications are needed to account for the different nature of the dominant scattering mechanisms and consequently the nonlinearities are much more pronounced due to the relatively larger contribution of quasi-specular reflexion versus Bragg scattering.

This paper explores the spatial variability of the SAR-derived directional wave spectrum from a coastal SAR scene in which the oceanic swell may be considered to be homogeneous but there is a strongly heterogeneous wind field. The aim is to investigate the extent to which the variable wind speed and direction alters the SAR retrieved swell wave spectrum, and also to try to shed some light into the discussion of the effect of swell on the wind sea part of the spectrum. We assume as a first approximation that any difference between the spectra in the wind sheltered and non-sheltered areas could be related to a possible interaction between wind sea and swell, since the wind sea part of the spectrum would show slightly different values of wave height and mean period due to the different wind speeds.

## 2. Data and methods

### 2.1. SAR measurements

The retrieval algorithm for SAR Wave Measurements is the Max Planck Institute (MPI) scheme (Hasselmann et al., 1996),

adapted in this work to use as input a SAR Precision Image instead of the SWM. The mapping of an ocean wave spectrum  $F(\mathbf{k})$  onto a SAR image spectrum  $P(\mathbf{k})$  (Hasselmann and Hasselmann, 1991) is a closed integral transform in the form

$$P(\mathbf{k}) = \exp(-k_a^2 \zeta^2) \sum_{n=1}^{\infty} \sum_{m=2n-2}^{2n} (k_a \beta)^m P_{nm}(\mathbf{k}) \quad (1)$$

where  $\exp(-k_a^2 \zeta^2)$  describes an exponential fall-off of the spectrum beyond an azimuthal cut-off wavenumber. This term can be thought of as a low-pass filter where the information beyond the cut-off is suppressed. The SAR imaging mechanism is strongly nonlinear due to distortions induced by the orbital wave motions (the velocity bunching mechanism) causing degradation of the azimuthal (parallel to the satellite flight) resolution. The result of this distortion is that there is a loss of information beyond a cut-off wavenumber and waves with wavelengths shorter than 150–200 m propagating in the azimuthal direction are not mapped onto the SAR image directly. The root mean square azimuthal displacement is given by  $\zeta^2 = (u_r \beta)^2 = \beta^2 \int |T_k|^2 F(\mathbf{k}) d\mathbf{k}$ , where  $\beta$  is the ratio of the slant range to the platform velocity  $R/V$ ,  $u_r$  is the orbital velocity and  $T_k$  is the velocity bunching modulation transfer function.  $P_{nm}$  represents the Fourier transform of the auto and cross-covariance functions of the Real Aperture Radar image intensity and the orbital velocity, and the indexes  $n$  and  $m$  indicate, respectively, the order of nonlinearity with respect to the input wave spectrum and the velocity bunching mechanism.

The MPI scheme finds a retrieved wave spectrum by cost-function minimization, which depends on a first guess wave spectrum, the SAR input spectrum and the azimuthal cut-off wavenumber. The full nonlinear mapping relation (1) is used to calculate the SAR image spectrum from a first guess wave spectrum. In the present study the first guess wave spectrum is from the archives of the National Centers for Environmental Prediction/National Oceanic and Atmospheric Administration (NCEP/NOAA) WW3 model (Tolman, 1991) with specific point output that corresponds to locations where NDBC (National Data Buoy Center) buoys report data (see NCEP/NOAA, 2010). The retrieval of wave spectra from SAR images requires the first guess wave spectrum to solve the directional ambiguity and to extend the spectral information beyond the high wavenumber cut-off caused by nonlinearities in the imaging process. The inversion is achieved when the difference between two iterations is smaller than a specific value. The form of the spectrum is modified only up to the point where there is SAR spectral information and beyond the cut-off wavenumber it retains the information from the first guess wave spectrum—more details in Hasselmann et al. (1996) and Violante-Carvalho et al. (2005).

Only the wave components in the low frequency part of the spectrum are visible on SAR images whereas the high frequency information yielded by the retrieval is derived from the wave model. Therefore, only the swell systems are directly measured by SAR.

The study area covers a region of the coastal Pacific Ocean off Monterey Bay, California (Fig. 1), and the SAR scene used for this study is from ERS-2 (Fig. 2). It was divided into 6.4 km square sub-images for separate wave spectral analysis. The processing of the  $512 \times 512$  pixels sub-images follows the description in ESA (1995). In short, the 2D image power spectrum is calculated applying a Hamming window and a 2D FFT is performed, the spectrum converted from complex to real space and normalized. Then it is transformed from cartesian to polar coordinates and saved in the UWA format (ESA, 1995). The image spectrum is used as an input for the MPI retrieval algorithm, as well as the first guess wave spectrum from the NCEP/NOAA WW3 model.

SAR has the capability of high-resolution imaging so that detailed distribution of wind vectors can be retrieved. The calibrated normalized radar cross-section is a nonlinear function

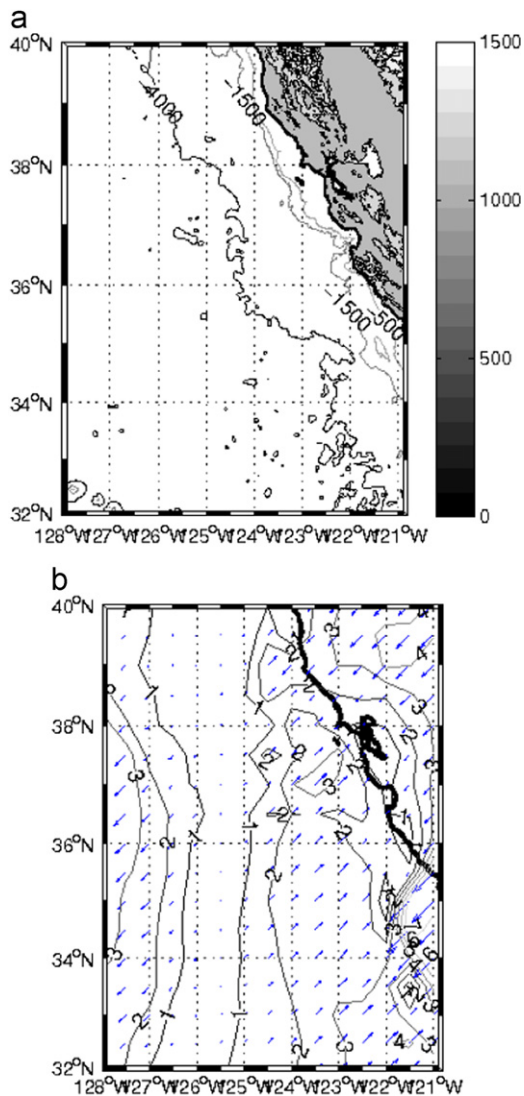


**Fig. 1.** (a) Map of the topography and bathymetry of the study area. (b) Wind field at 10 m height with resolution of  $0.5 \times 0.5^\circ$  from Quikscat (QSCAT/NCEP Blended Ocean Winds) on November 3, 2007, at 1800 UTC.

of wind speed through the dominant Bragg scattering mechanism at moderate angles of incidence. To extract the surface wind information from SAR data requires a geophysical model function, such as the C-band model function (see, for example, Alpers et al., 1981; Hasselmann et al., 1985; Horstmann et al., 2000; Isoguchi and Kawamura, 2007). Several algorithms have been developed and applied to derive the surface wind field from SAR images, such as the CMOD5 model (Hersbach et al., 2007).

However, at low wind speed, the performance of the geophysical model functions for inverting wind speed based on backscatter has been varied. Our attempts to apply the CMOD5 model to the image presented in Fig. 2 have not given a reliable wind field. Monterey Bay is protected from the offshore coastal winds by the mountains. Therefore one would expect that, during the events that we are selecting, low wind conditions will prevail, which makes more difficult the retrieval of the very high resolution SAR wind field.

## 2.2. Buoy measurements

Wind and directional wave measurements were made by the NDBC buoy station 46042 moored in a depth over 1500 m at

position  $36^\circ 47' 19''\text{N}$  and  $122^\circ 24' 15''\text{W}$  (Fig. 2b), off Monterey Bay, California (more details see NOAA/NDBC, 2010). The buoy data of the 3 m diameter discus hull is made available for continuous sets of hourly wind and directional wave data.

Wind speed (m/s) is averaged over an eight-minute period, with the same averaging period for wind direction (direction the wind is coming from in degrees clockwise from true N). The anemometer is located approximately 5 m above the waterline, and the wind speed is not adjusted to the standard 10 m height. The directional spectrum, and therefore the significant wave height, is calculated during the 40-min sampling period of the buoy.

## 3. Results

The map with land topography and bathymetry based on the Etopo data set and the surface wind field derived with QuickScat/NCEP Blended data are presented in Fig. 1. The wind field, at 10 m height, has spatial resolution of  $0.5 \times 0.5^\circ$ , with time difference between the SAR passage of approximately 50 min. This area is particularly interesting because of the NDBC directional wave buoys moored in deep water near a hilly coast, and an event of offshore winds was selected from the European Space Agency catalogue of SAR images.

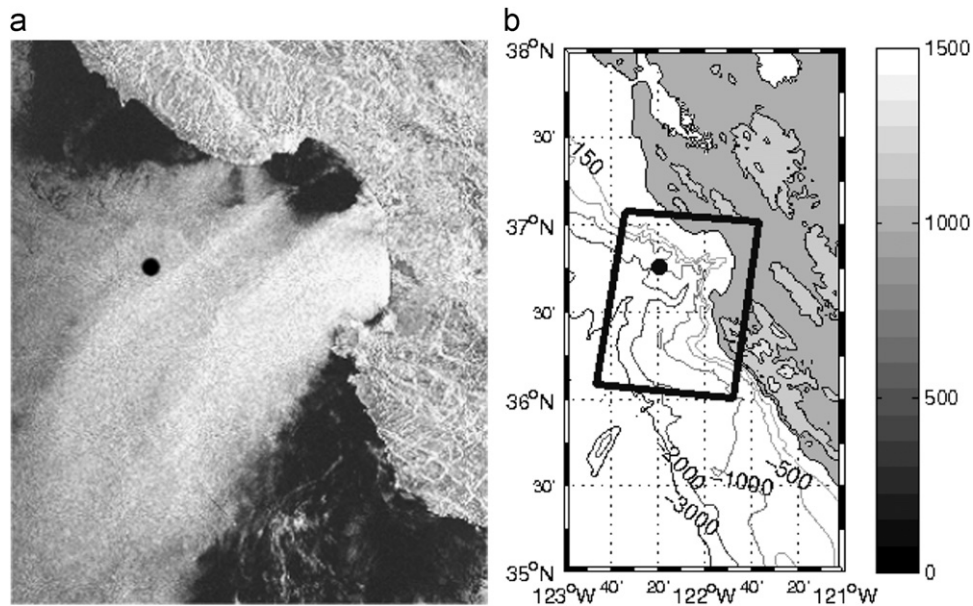
Fig. 2 is the quick look of the ERS-2 SAR precision image and a zoom of the area around the buoy, with part of Monterey Bay located on the top right corner of the image. As indicated in Fig. 1b, the wind flows from land to sea over a hilly area, with mountains higher than 1000 m. The features of the SAR image (Fig. 2a) suggest that the sheltering effect of the mountains causes regions with different surface wind speeds over the coastal oceanic region.

Fig. 3 shows the recent history of the buoy measurements of wind and wave height in the 8 days leading to the time of the SAR acquisition. The wind was persistent from the east-northeast for about 10 h before the image acquisition, while its speed was around 5 m/s. It is also worth noting that there is no significant change in wave height during the interval while the wind was flowing from land to sea.

To retrieve wave spectra over different areas of wind speed, sub-images are selected, shown in Fig. 4. The upper part of the gridded image is darker, with lighter winds, caused by the sheltering effect of the mountains. For some of the sub-images displayed in Fig. 4, the retrieval did not yield a wave spectrum, perhaps because of noise in some parts of the image. The retrieval accuracy is reduced when one looks at low wind speeds, ranging between 1 and 5 m/s (Alpers et al., 1981), which is the present case.

It is assumed that, over such a relatively small area (of the selected sub-images, about  $50 \text{ km} \times 80 \text{ km}$ ) located in deep water, the swell is homogeneous. This seems to be a robust assumption. The mean period of the swell components that we are interested in is over 10 s. Their generation area might well be located several hundred miles away. Hence, it is reasonable to assume that, through frequency dispersion and directional spreading, their propagation to the study area will result in homogenization of the wave field located in deep water. Therefore, any significant spectral change would be related to local conditions, such as a heterogeneous wind field or a non-uniform wind sea component.

Fig. 5 displays the NCEP/NOAA WW3 spectrum used as first guess for the inversion, alongside the buoy spectrum. The wind is blowing from the east-northeast (the wind sea component is west-northwestward). The buoy spectrum has a wind sea and two swell components, north-westward and south-eastward. The wind sea component and the more energetic south-eastward swell component are propagating in almost opposite directions.



**Fig. 2.** (a) Quick look (8 by 8 pixels average) of the ERS-2 SAR PRI (Precision Image) on November 3, 2007, at 1849 UTC. The black dot represent NDBC Buoy 46042. (b) Topography and bathymetry of the area around NDBC Buoy 46042 (also represented as a black dot), and the location of the ERS-2 SAR image used in the study.

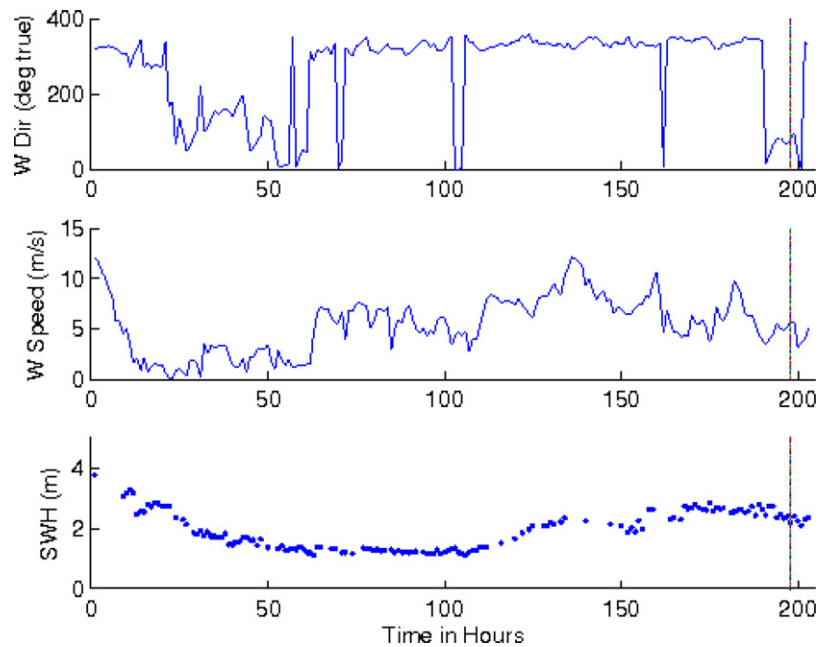


**Fig. 3.** Respectively from top to bottom, time history of wind direction, wind speed and significant wave height measured by the buoy during the 8 days prior to the time of acquisition of the SAR Image, also shown as vertical lines.

The WW3 model, on the other hand, was not able to estimate properly either the wind sea component or the north-westward swell, despite the good agreement between measured and estimated significant wave heights. To examine a possible interaction among short and long wind waves, we focus on the south-eastward swell component, since the less prominent north-westward swell is, comparatively, more difficult to pick out.

A partitioning scheme for decomposing the two-dimensional directional wave spectrum into its distinct components, wind sea and swell, was originally proposed by Gerling (1992). Hasselmann et al. (1996), based on his work, presented a modified partitioning algorithm to compare SAR and model wave spectra. A further adaptation of the spectral 2D partitioning scheme, described in Violante-Carvalho et al. (2005), is here employed. An example of

the partitioning of the retrieved SAR wave spectra, corresponding to one of the sub-images depicted in Fig. 4, is shown in Fig. 6. Furthermore, the 1D spectra are obtained by integrating the partitioned 2D south-eastward wave spectrum (buoy and retrievals from SAR) over direction.

The 1D SAR wave spectra are computed for each sub-image over the sheltered and non-sheltered regions in Fig. 4. The averaged SAR wave spectra (solid line in Fig. 7a and b) are presented together with the buoy spectrum (dashed line in Fig. 7a and b). The standard deviations of the peak energy and peak frequency are also shown, as vertical and horizontal bars. It is clear that the variability of the peaks of the spectra retrieved over both regions overlaps, so apparently there is no clear difference in the swell energy regarding the different wind sea

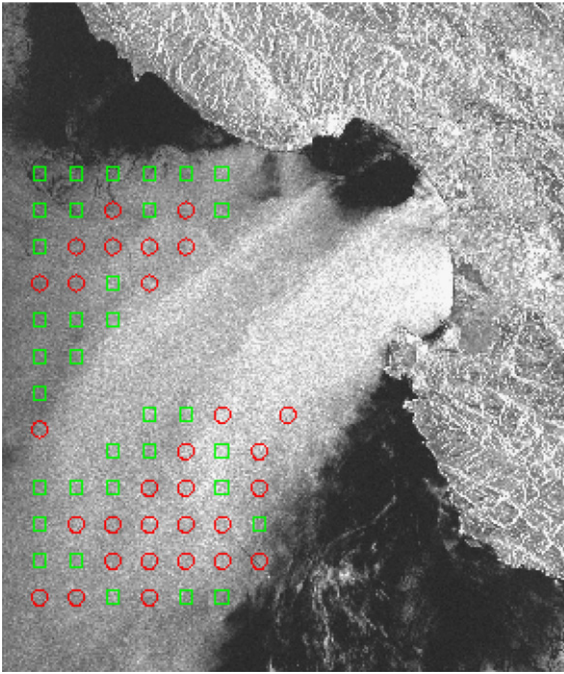


**Fig. 4.** Sub-images ( $6.4 \times 6.4$  km, 512 pixels each side) over two areas located in deep water with regional difference of wind speed. In some of the sub-images, the wave spectra were not retrieved properly (red circles), while those that the retrieval scheme was successful are represented as green squares. (For interpretation of the references to color in this figure legend, the reader is referred to the web version of this article.)

components. There is either no clear evidence on any change in the swell wavelength over the sheltered and non-sheltered regions. Only average values are shown and only for one image.

Sun and Kawamura (2009) performed a similar investigation employing an ERS-1 SAR image off Kii Peninsula, Japan, searching for possible modifications on the wave field associated with a non-homogeneous wind field. In their work, they applied equation (1) to retrieve the swell spectrum, which was assumed homogenous over the SAR image formed by a strong wind front caused by the sheltering effect of the islands. They observed a more pronounced wind speed contrast along the front, with higher wind speeds, about 9 m/s in the sheltered region and about 12 m/s in the non-sheltered region. Their analysis point out that the derived SAR wavelength is longer in the sheltered area than in the non-sheltered area. The energy level of the swell spectrum, according to their results, is lower in the region with lighter winds, and slightly higher in the non-sheltered area. That work did not attempt to draw any conclusions about the possible causes of the modifications observed in the swell component.

#### 4. Summary and conclusions

We have examined in this work the spatial homogeneity of SAR wave spectra retrieved from an ERS-2 Precision Image. The image was acquired of the coastal Pacific Ocean off Monterey Bay, California, with winds blowing from the east quadrant, from land to ocean. The sheltering effect of the mountains formed coastal regions with different surface wind speeds over the SAR image, and we have investigated the possible interaction of long waves with short waves.

Applying a partitioning scheme, different wave systems were isolated from the 2D spectra retrieved from the SAR and measured by a directional buoy moored nearby. It is assumed that a swell component is homogeneously present over the image, and

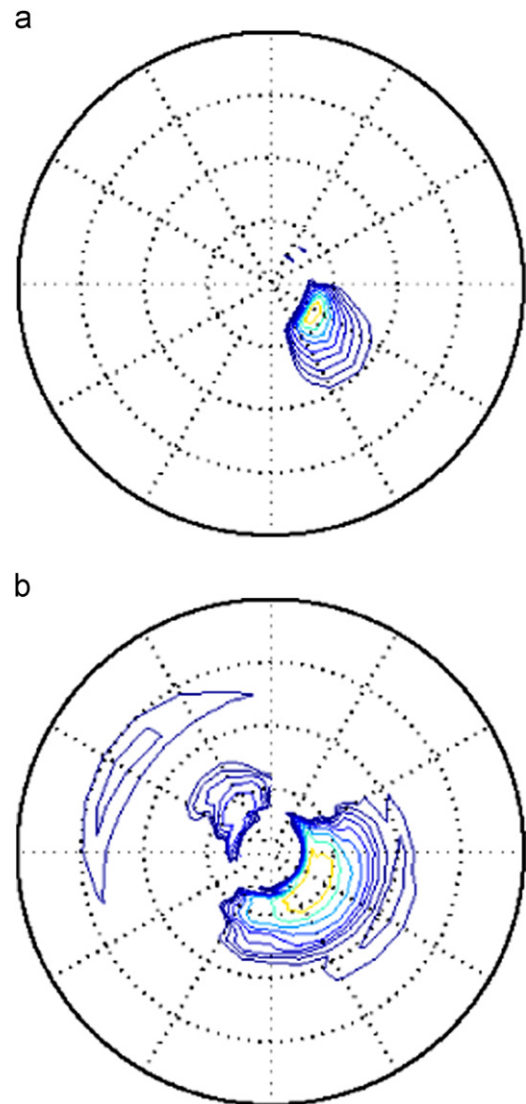


**Fig. 5.** Spectra in polar frequency-directional plots. Circles denote frequency at 0.1 Hz interval from 0.1 Hz (inner circle) till 0.4 Hz (outer circle). Isolines are logarithmically spaced relative to the maximum value of the spectral energy density. Panel (a) is the NOAA WW3 directional spectrum used as a first guess for the inversion. Significant wave height of 2.4 m, mean period of 10.8 s, wind speed  $U_{10} = 2.8$  m/s and wind direction  $85.5^\circ$  true. (b) is the NDBC buoy 46042 spectrum, with significant wave height of 2.2 m, peak period of 10.8 s, wind speed  $U_{10} = 5.6$  m/s and wind direction  $82^\circ$  true.

several sub-images were selected over the areas with regional difference of wind speed. From the sub-images, SAR wave spectra were retrieved and intercompared to examine any possible influence of the wind on the swell propagation.

There is no evident difference among the averaged spectra computed over the sheltered and non-sheltered regions in our study case, with the two spectra being identical within sampling variability. Therefore our measurements indicate that there is no significant effect of the variable wind speed on the swell component. However, there seems to be a small increase in swell energy in the non-sheltered area (Fig. 7b), where there is stronger surface winds and therefore a more energetic wind sea component. This tendency seems to corroborate the results obtained by Sun and Kawamura (2009) in a higher wind situation.

A stronger wind sea part of the spectrum will exhibit a stronger nonlinear interaction, with more energy transfer from high to low frequency bands. However, in the particular situation investigated in this work, it seems unlikely to be the case. The

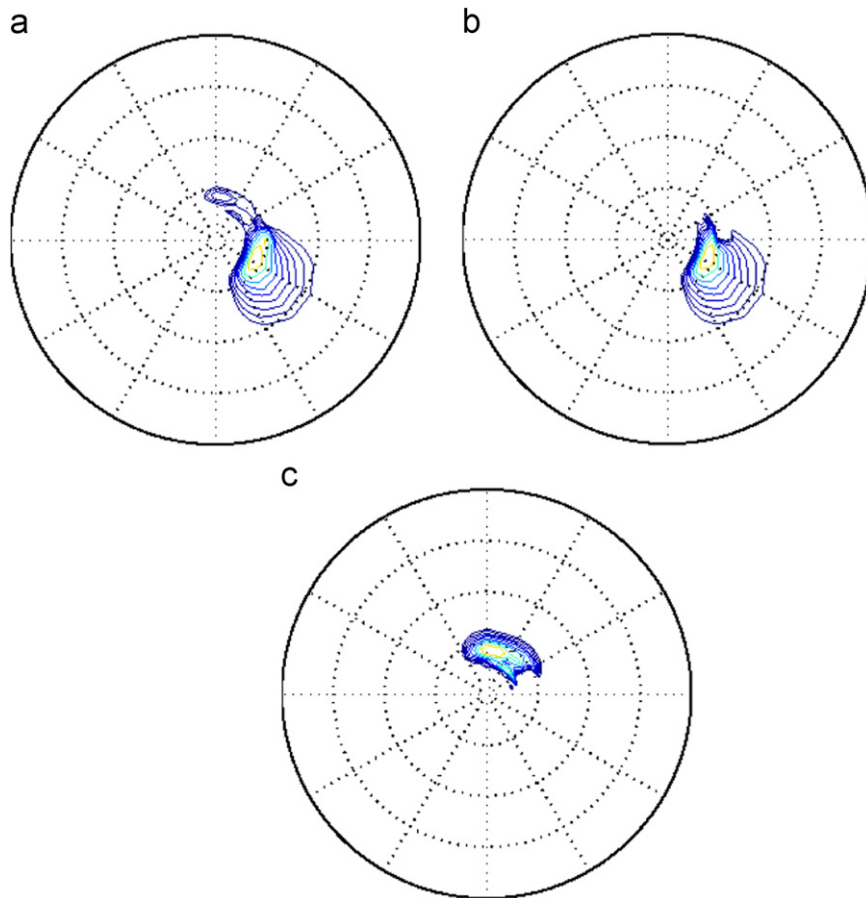


**Fig. 6.** Example of the partitioning of the 2D SAR wave spectrum. Panel (a) is the full spectrum, while (b) and (c) are its separated wave component.

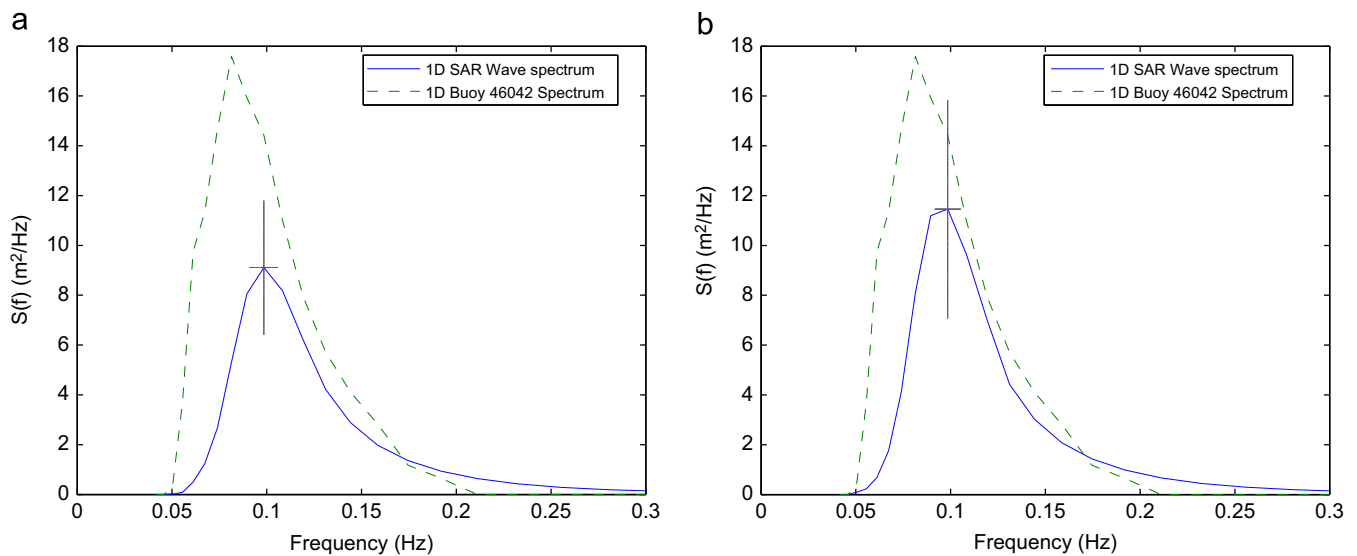


**Fig. 7.** The 1D wave spectra of the swell component propagating south-eastward in Fig. 5, the dashed line is the one measured by the buoy and the solid line the one retrieved by the SAR. Panel (a) shows the averaged 1D wave spectrum in the darker region in Fig. 4, while (b) is the averaged 1D wave spectrum in the lighter region. Also shown, the standard deviations of the peak energy and peak frequency, respectively the vertical and horizontal bars.

wind sea and swell components are relatively distant in frequency space, propagating in almost opposite directions, which would make the nonlinear interactions less significant. On the other hand, the swell component is propagating against the wind. Although there are some evidences about the effect of swell on the growth of wind waves, there are no conclusive studies about

any significant increase in swell height by extracting energy from an opposing wind.

Another question that could be raised is whether any possible difference be an artefact of the extra radar scattering due to the higher Bragg wave energy in the windier areas. In other words, the swell may be the same, but the SAR modulation processes

measure the swell differently because of the extra Bragg roughness. If so it would question the fundamental assumptions about swell spectral retrieval from SAR. The answer would require separate in situ buoys sampling the different areas to confirm whether the swell itself is different in the two areas.

Nevertheless, despite the fact that our results give some evidence that there is no strong effect of shorter waves on longer waves, the variability of the retrieved spectra makes it difficult to draw any definite conclusions from this single case study. It will be worth analysing further scenes of a similar character to determine whether wind–swell interaction can be confirmed from a larger number of examples.

## Acknowledgments

The ERS-2 SAR image was obtained from the European Space Agency, through Category-1 Proposal 6401 (C1P.6401). NVC was supported in part by the Brazilian National Research and Development Council (CNPq) under Grant PDE 201197/2008-1.

## References

- Alpers, W.R., Ross, D.B., Rufenach, C.L., 1981. On the detectability of ocean surface waves by real and Synthetic Aperture Radar. *Journal of Geophysical Research* 86 (C7), 6481–6498.
- Ardhuin, F., Chapron, B., Collard, F., 2009. Observation of swell dissipation across oceans. *Geophysical Research Letters* 36. doi:10.1029/2008GL037030.
- Chen, G., Belcher, S.E., 2000. Effects of long waves on wind-generated waves. *Journal of Physical Oceanography* 30, 2246–2256.
- Collard, F., Ardhuin, F., Chapron, B., 2005. Extraction of coastal ocean wave fields from SAR images. *IEEE Journal of Oceanic Engineering* 30 (3), 526–533.
- Dobson, F., Perrie, W., Toulany, B., 1989. On the deep-water fetch laws for wind-generated surface gravity waves. *Atmosphere-Ocean* 27 (1), 210–236.
- Donelan, M.A., 1987. The effect of swell on the growth of wind waves. *Johns Hopkins APL Technical Digest* 8(1), pp. 18–23.
- ESA, 1995. European Space Agency, ERS-1&2 UWA Processing Algorithm Specification. Disponível em: [earth.esa.int/pub/ESA\\_DOC/UWA/er\\_tn\\_es.pdf](http://earth.esa.int/pub/ESA_DOC/UWA/er_tn_es.pdf). Acesso em maio de 2010.
- García-Nava, H., Ocampo-Torres, F.J., Osuna, P., Donelan, M.A., 2009. Wind stress in the presence of swell under moderate to strong wind conditions. *Journal of Geophysical Research* 114. doi:10.1029/2009JC005389.
- Gerling, T., 1992. Partitioning sequences and arrays of directional ocean wave spectra into component wave systems. *Journal of Atmospheric and Oceanic Technology* 9, 444–458.
- Hanson, J.L., Phillips, O.M., 1999. Wind sea growth and dissipation in the open ocean. *Journal of Physical Oceanography* 29, 1633–1648.
- Hasselmann, K., Hasselmann, S., 1991. On the nonlinear mapping of an ocean wave spectrum into a Synthetic Aperture Radar image spectrum and its inversion. *Journal of Geophysical Research* 96 (C6), 10,713–10,729.
- Hasselmann, K., Raney, R.K., Plant, W.J., Alpers, W., Shuchman, R.A., Lyzenga, D.R., Rufenach, C.L., Tucker, M.J., 1985. Theory of synthetic aperture radar ocean imaging: a MARSEN view. *Journal of Geophysical Research* 90 (C3), 4659–4686.
- Hasselmann, S., Brüning, C., Hasselmann, K., Heimbach, P., 1996. An improved algorithm for the retrieval of ocean wave spectra from Synthetic Aperture Radar image spectra. *Journal of Geophysical Research* 101 (C7), 16,615–16,629.
- Hersbach, H., Stoffelen, A., de Haan, S., 2007. An improved C-band scatterometer ocean geophysical model function: CMOD5. *Journal of Geophysical Research* 112. doi:10.1029/2006JC003743.
- Horstmann, J., Koch, W., Lehner, S., Tonboe, R., 2000. Wind retrieval over the ocean using synthetic aperture radar with C-band HH polarization. *IEEE Transactions on Geoscience and Remote Sensing* 38 (5), 2122–2131.
- Isoguchi, O., Kawamura, H., 2007. Coastal wind jets flowing into the Tsushima Strait and their effect on wind-wave development. *Journal of the Atmospheric Sciences* 64 (2), 564–578.
- Krogstad, H.E., Samset, O., Vachon, P.W., 1994. Generalizations of the non-linear ocean-SAR transform and a simplified SAR inversion algorithm. *Atmosphere-Ocean* 32 (1), 61–82.
- Masson, D., 1993. On the nonlinear coupling between swell and wind waves. *Journal of Physical Oceanography* 23, 1249–1258.
- Mastenbroek, C., de Valk, C.F., 2000. A semiparametric algorithm to retrieve ocean wave spectra from Synthetic Aperture Radar. *Journal of Geophysical Research* 105 (C2), 3497–3516.
- Mitsuyasu, H., Yoshida, Y., 2005. Air–sea interactions under the existence of opposing swell. *Journal of Oceanography* 61 (1). doi:10.1007/s10872-005-0027-1.
- NCEP/NOAA, 2010. National Centers for Environmental Prediction/National Oceanic and Atmospheric Administration. Available in <<http://polar.ncep.noaa.gov>>. Accessed in May 2010.
- NOAA/NDBC, 2010. National Oceanic and Atmospheric Administration/National Data Buoy Center. Available in <<http://www.ndbc.noaa.gov>>. Accessed in May 2010.
- Phillips, O.M., Banner, M.L., 1974. Wave breaking in the presence of wind drift and swell. *Journal of Fluid Mechanics* 6 (Part 4), 625–640.
- Schulz-Stellenfleth, J., Lehner, S., Hoja, D., 2005. A parametric scheme for the retrieval of two-dimensional ocean wave spectra from synthetic aperture radar look cross spectra. *Journal of Geophysical Research* 110 (C5), C05004.
- Sun, J., Kawamura, H., 2009. Modification of SAR spectra associated with surface wind fields in the sea off the Kii Peninsula: a case study. *Journal of Oceanography* 65, 45–52.
- Tolman, H., 1991. A third-generation model for wind waves on slowly varying, unsteady and inhomogeneous depths and currents. *Journal of Physical Oceanography* 21, 782–797.
- Violante-Carvalho, N., Ocampo-Torres, F.J., Robinson, I.S., 2004. Buoy observations of the influence of swell on wind waves in the open ocean. *Applied Ocean Research* 26 (1–2), 49–60.
- Violante-Carvalho, N., Robinson, I.S., Schulz-Stellenfleth, J., 2005. Assessment of ERS Synthetic Aperture Radar wave spectra retrieved from the MPI scheme through intercomparisons of one year of directional buoy measurements. *Journal of Geophysical Research* 110 (C07019).
- Young, I.R., Verhagen, L.A., Banner, M.L., 1995. A note on the bimodal directional spreading of fetch-limited wind waves. *Journal of Geophysical Research* 100 (C1), 773–778.